crystals

MDPI

Article

Structure and Thermal Stability of Two Estetrol Solvates

Magda Monari [1], Emanuele Attolino [2], Gianfranco Lopopolo [2], Fabrizio Bosco [2] and Massimo Gazzano [3,*]

[1] Dipartimento di Chimica "G. Ciamician", University of Bologna, Via Selmi 2, 40126 Bologna, Italy; magda.monari@unibo.it
[2] NEWCHEM SpA, Via San Vittore 39, 20123 Milano, Italy; emanuele.attolino@newchemspa.it (E.A.); gianfranco.lopopolo@newchemspa.it (G.L.); fabrizio.bosco@newchemspa.it (F.B.)
[3] Institute for Organic Synthesis and Photoreactivity (ISOF), CNR, Via Gobetti 101, 40129 Bologna, Italy
* Correspondence: massimo.gazzano@isof.cnr.it

Abstract: Two solvates of estetrol have been isolated and characterized by SCXRD and PXRD as well as by thermal analyses, morphology and spectroscopy. Estetrol monohydrate (Estetrol.H_2O, S.G. P1, Z = 12) contains 12 molecules in its asymmetric unit with very subtle conformational differences with one another but reveals an intricate network made of intermolecular H-bonds established with the neighbour estetrol molecules and with crystallization water. Each molecule of estetrol methanol hemisolvate (Estetrol.0.5CH_3OH, S.G. C2, Z = 4) establishes six O-H. . .O bonds with six different neighbours and additional H-bonds with methanol. In both structures, estetrol molecules are organized in a head-to-tail arrangement that favours the formation of O-H. . .O interactions. The increased thermal stability of Estetrol.0.5CH_3OH crystals with respect to Estetrol.H_2O can be correlated to the strengthened network of H-bonds.

Keywords: estetrol; polymorphism; crystal structure; thermal stability

check for updates

Citation: Monari, M.; Attolino, E.; Lopopolo, G.; Bosco, F.; Gazzano, M. Structure and Thermal Stability of Two Estetrol Solvates. *Crystals* **2023**, *13*, 1211. https://doi.org/10.3390/cryst13081211

Academic Editors: Małgorzata Hołyńska and Ionut Tranca

Received: 21 July 2023
Revised: 2 August 2023
Accepted: 3 August 2023
Published: 5 August 2023

1. Introduction

Drug polymorphism is of special importance either because of its great impact on physicochemical and biological properties, or because of its effect on authorization processes and the patentability of active pharmaceutical ingredients. Because both these aspects strongly influence industrial applications, the possibility to have different crystal forms or the solvated ones, generically named pseudopolymorphs, are at present accurately scouted.

Estetrol (E4, Scheme 1), is one of the few steroids endowed with estrogenic activity naturally present in humans. It is produced in foetal liver and is therefore also present in the body of pregnant women during the foetal phase. Its level in the body dramatically decreases after birth [1]. It was discovered in 1965 [2] but started to receive great attention only in the last 20 years, as demonstrated by several studies focused on the potential clinical use of the estrogenic activity of the molecule [3].

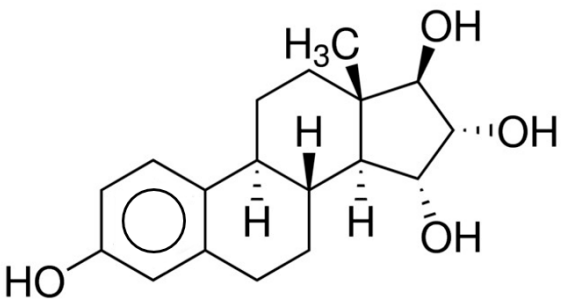

Scheme 1. The estetrol molecule.

The growing interest has been mainly due to the high selectivity of estetrol for the estrogen receptor [4–6], determining its great potential for the development of low-risk

hormone therapy. In particular, estetrol has been mainly evaluated as a strategic alternative to the synthetic estrogen Ethinylestradiol, commonly used as an oral contraceptive, in combination with a progestinic derivative, with lower risks of venous thromboembolism as well as reduced side effects at the level of breast and liver [7–10].

Recently, a new oral contraceptive based on a combination of estetrol and drospirenone has been approved by several regulatory authorities in the world including those of Europe, the United States, Canada and Australia, and the drug is commercially available [11].

Besides birth control, additional pre-clinical and clinical trials are currently in progress for other therapeutic applications of estetrol, such as the treatment of post-menopausal symptoms and cancer as well as in neuroprotection and dermatology [12–18], confirming the great attention of the international scientific community for this molecule, already highlighted as 'molecule of the week' by ACS [19].

Even if estetrol is a naturally occurring steroid, the Active Pharmaceutical Ingredient (API) industrial production is performed via chemical synthesis starting from Estrone. Several industrial manufacturing processes have been reported so far in patent literature making use of batch production methods [20–24] also via biochemical transformation [25], and very recently the use of flow chemistry for the production of a key intermediate of the estetrol has been published [26].

Depending on the crystallization conditions, the solid pure API can be isolated both as crystalline monohydrate and anhydrous forms [27]; the monohydrate one is the crystal form currently used for formulation, but a crystal structure is not reported for any of them.

Once the crystalline form used for the formulation of the API has been selected, it is good practice, for synthetic chemists involved in the development of the industrial manufacturing process, to evaluate if the crystal form used for formulation can be useful also for the purification of the crude product coming from the synthesis, in order to match the regulatory specifications of the API. As previously explained, estetrol has been recently approved and an international pharmacopoeia is not available yet for this product. For this reason, in our laboratory, the specifications suggested by the International Council for Harmonisation (ICH) guidelines were selected. Unfortunately, in our hands, the anhydrous form of estetrol did not appear to be a proper crystal in order to match the specifications, and, also, a certain hygroscopicity of the solid was evidenced. For this reason, we preferred to isolate crude estetrol essentially as a hydrate form and to develop a final crystallization yielding the regulatory pure monohydrate form. During attempts to evaluate in our laboratories the best solvent mixture and identify the correct experimental conditions to perform the industrial crystallization of the API, a new stable crystalline solvate form of estetrol was discovered.

In this study, the thermal stability, crystal structure, morphology, and spectroscopic properties of estetrol monohydrate (Estetrol.H_2O) will be compared to those of the newly discovered methanol hemisolvate (Estetrol.0.5CH_3OH) crystalline form. The investigation was performed via DSC, TGA, temperature-variable XRD, single-crystal diffraction and IR spectroscopy.

2. Materials and Methods

2.1. Chemicals

Estetrol was synthesized following well-known procedures [28] in Newchem's R&D laboratories. Solvents used for the crystallization methods were of analytical grade and purchased from Merck company (Merck KGaA, Darmstadt, Germany).

2.2. Thermal Analysis

Differential scanning calorimeter (DSC) scans were carried out by using a TA-Q20 instrument (TA Instruments, New Castle, DE, USA), following a temperature increase of 10 °C/min, from 35 °C up to 350 °C with a nitrogen flow of 50 mL/min. Thermogravimetric analysis (TGA) was carried out using a TA-Q500 instrument. Heating was performed in a

platinum crucible with nitrogen flow (sample gas 60 mL/min; balance gas 40 mL/min) at a rate of 10 °C/min, from 35 °C up to 550 °C.

2.3. IR Spectroscopy

IR spectra were carried out by using a Perkin Elmer Spectrum Two FT-IR spectrometer (Perkin Elmer, Waltham, MA, USA), equipped with a UATR TWO device for attenuated total reflectance acquisition. Data were recorded with a resolution of 4 cm^{-1}, and 32 scans were averaged for each spectrum between 4000 cm^{-1} and 650 cm^{-1}. As a reference, the background spectrum of air was collected before the acquisition of each sample spectrum.

2.4. Structural Investigation PXRD

X-ray diffraction (XRD) patterns of microcrystalline/powder samples were carried out by using a PANalytical X'PertPro (Malvern Panalytical, El Almelo, The Netherlands) diffractometer equipped with a copper target (λ = 0.15418 nm) and a fast solid state X'Celerator detector. Data were recorded in the 3–60° 2 theta interval, by collecting 25 s at each step (0.05°). Collection of XRD data in situ at variable temperatures was performed with a TTK450 Anton Paar device, heating at 20 °C/min and keeping isothermal conditions during XRD scanning.

2.5. Single Crystal Crystallography SCXRD

Crystals of Estetrol.H_2O and Estetrol.0.5CH_3OH suitable for SCXRD studies were mounted on a loop with Fomblin©protective oil. The X-ray intensity data for Estetrol.H_2O and Estetrol.0.5CH_3OH were collected on a Bruker D8 Venture single crystal X-ray diffractometer (Bruker AXS Inc., Madison, WI, USA) coupled with a Photon III area detector using Cu−Kα radiation at −173 °C. All data were processed using the Bruker suite of programs [29–31] and the structures were solved using direct methods and refined with a full-matrix least-squares fitting on F^2 using the SHELX program suite [32,33].

All non-hydrogen atoms were assigned anisotropic displacement parameters. Most of the hydrogen atoms, except the H atoms of the solvent water molecules in Estetrol.H_2O, were located in the Fourier map, placed in idealized positions and included as riding with constrained isotropic displacement parameters (C-H = 0.98, 0.99, 1.00 and 0.98 Å for methyl, methylene, methine and aromatic protons, respectively), and refined as riding with Uiso (H) = 1.2 or 1.5Ueq (Cmethyl). The positions of the O-H hydrogens were found in the Fourier maps in both structures and refined using a riding model.

Estetrol.H_2O gives only small crystals despite many attempts of growing larger and better-quality crystals and a few of them were tried before starting the data collection. All of them gave the same triclinic unit cell (S.G. 1) that contains 12 independent molecules and 12 crystallization water molecules. The structure model has undergone several refinement cycles in order to look for a second image for C16, C15, O3 and O2 of G molecule which show abnormally elongated thermal displacement ellipsoids (that were refined isotropically) but no significant electron density peak was detected in the Fourier map in the vicinity of the aforementioned atoms. Presumably the crystal quality prevents us from understanding the nature of the disorder.

In Estetrol.0.5CH_3OH, the methanol molecule is disordered across a twofold rotation axis. Molecular graphics were generated using the Mercury program [34]. Table 1 reports crystal data and refinement parameters for the two structures. CCDC 2277249 (Estetrol.H_2O) and CCDC 2277250 (Estetrol.0.5CH_3OH) contain the crystallographic data for this paper (accessed on 27 June 2023) [35].

Table 1. Crystal data and structure refinement for Estetrol.H_2O and Estetrol.0.5CH_3OH.

Compound.	**Estetrol.H_2O**	**Estetrol.0.5CH_3OH**
Formula	$C_{18}H_{24}O_4.H_2O$	$C_{18}H_{24}O_4.0.5CH_3OHHHH$
Fw	322.39	320.39
T, K	100	100
λ, Å	1.54178	1.54178
Crystal symmetry	Triclinic	Monoclinic
Space group	*P*1	*C*2
a, Å	8.8822 (6)	18.9718 (5)
b, Å	23.7038 (15)	7.2471 (2)
c, Å	26.1126 (17)	13.8364 (4)
α, °	63.892 (3)	90
β, °	89.641 (3)	121.8010 (10)
γ, °	83.688 (3)	90
Cell volume, Å^3	4901.4 (6)	1616.79(8)
Z, *Z*′	12, 12	4, 1
D_c, Mg m^{-3}	1.311	1.316
M (Mo-K$_\alpha$), mm^{-1}	0.772	0.754
F (000)	2088	692
Crystal size/mm	0.10 × 0.05 × 0.03	0.35 × 0.35 × 0.10
θ limits, °	1.886 to 68.600	3.759 to 68.491
Reflections collected	143,487	21,309
Unique obs. Reflections [$F_o > 4\sigma(F_o)$]	34611 [R_{int} = 0.0782]	2934 [R_{int} = 0.0423]
Goodness-of-fit-on F^2	1.055	1.055
R_1 (F) [a], wR_2 [b] (F^2) [$I > 2\sigma(I)$]	0.0914 and 0.2434	0.0338 and 0.0830
Largest diff. peak and hole, e. Å^{-3}	1.034 and −0.704	0.393 and −0.326

[a] $R_1 = \sum||F_o| - |F_c||/\sum|F_o|$. [b] $wR_2 = [\sum w(F_o^2 - F_c^2)^2/\sum w(F_o^2)^2]^{1/2}$ where $w = 1/[\sigma^2(F_o^2) + (aP)^2 + bP]$, where $P = (F_o^2 + F_c^2)/3$.

3. Results and Discussion

3.1. Crystallization

Estetrol in monohydrate crystalline form was obtained via precipitation induced by the addition of water to a stirred clear solution of anhydrous estetrol in a 2-propanol–water mixture at room temperature. The suspension, thus obtained, was cooled to 0 °C and maintained under stirring at this temperature for one additional hour and then filtered, and the cake was washed with water. The wet solid was dried at 45 °C under a vacuum until the residual water content (monitored by Karl Fischer Titration) reached the range of 5.6 ÷ 5.7%.

Estetrol in methanol hemisolvate form was obtained by heating a dispersion of anhydrous estetrol in methanol until the complete dissolution of the steroid, followed by cooling to 0 °C. The resulting suspension was then stirred for 1 h at the same temperature and then filtered and washed with cold methanol. The wet solid was dried overnight under a vacuum at 50 °C.

3.2. Thermal Analysis

Measurements of the thermal evolution of two solvates are presented in Figure 1.

For Estetrol.0.5CH_3OH, TG-DTG analyses reveal a weight loss of −5.0 wt% corresponding to the removal of half of the molecules of methanol for each steroid molecule. The loss shows its maximum speed at 110 °C and thermal decomposition occurs at over 275 °C. The exhalation of one water molecule (−5.4 wt%) in the Estetrol.H_2O sample has its maximum gradient at 80 °C, and the weight loss due to decomposition starts at 260 °C. All the data indicate increased thermal stability of methanol solvate crystals with respect to monohydrate ones.

DSC scans exhibit two endothermic events. The second peak corresponds to the melting; it is sharp and occurs at 246 °C for both compounds with an exchange of 122 J/g. The first peak is at 111 °C for Estetrol.0.5CH_3OH sample and corresponds to the solvent

exhalation. In the Estetrol.H_2O sample, the peak is broad and asymmetric towards the lower temperatures. The peak is at 108 °C, a temperature much beyond that observed in TG for the water release. For this reason, we hypothesize the peak is the overlap of two endothermic events: the water loss at about 80 °C as evidenced in the TG scan and a structural transformation around 108 °C.

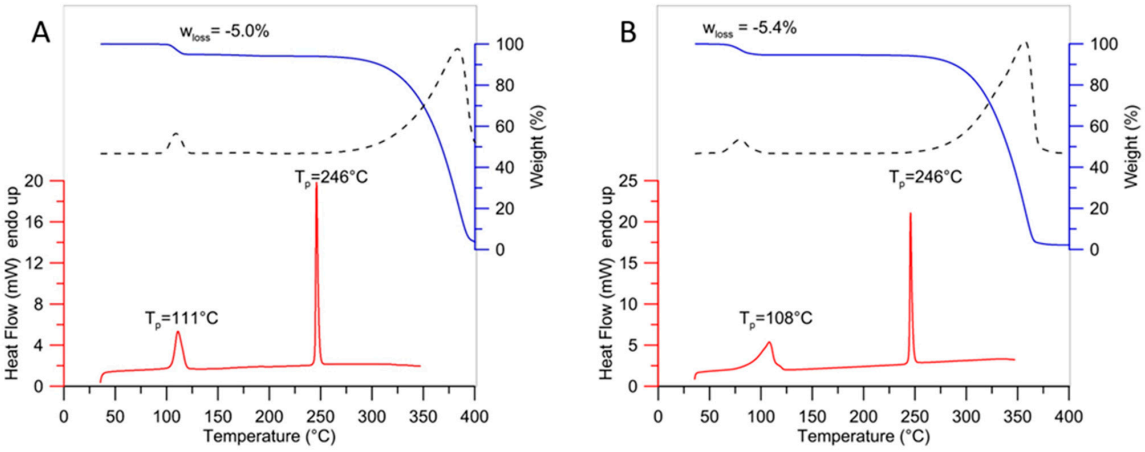

Figure 1. DTG-TG and DSC curves for Estetrol.0.5CH_3OH (**A**) and Estetrol.H_2O (**B**). Transition temperatures are reported as peak values.

3.3. Powder Diffraction

To gain more insight into structural aspects, samples were investigated via powder XRD. The patterns obtained at room temperature are reported in Figure 2a,c.

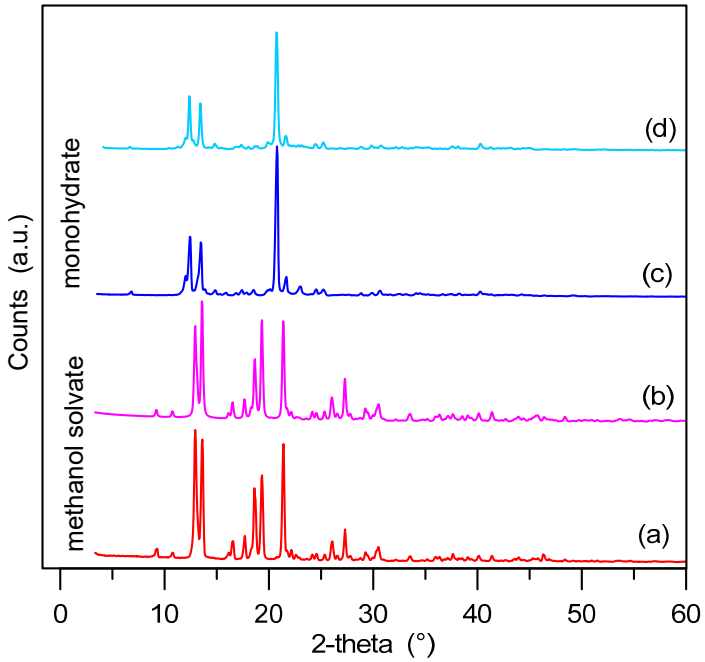

Figure 2. XRD patterns of Estetrol.0.5CH_3OH (**a**) and Estetrol.H_2O (**c**) samples. (**b**,**d**) are the respective patterns calculated from single-crystal data.

Both spectra are typical of fully crystalline material, but, since they differ in the number, position and relative intensity of the peaks, they belong to completely different structures. The two samples were also submitted to in situ XRD at variable temperatures in order to obtain patterns of each sample after the end of the first endothermic transformation associated with solvent removal. The patterns obtained are presented in Figure 3.

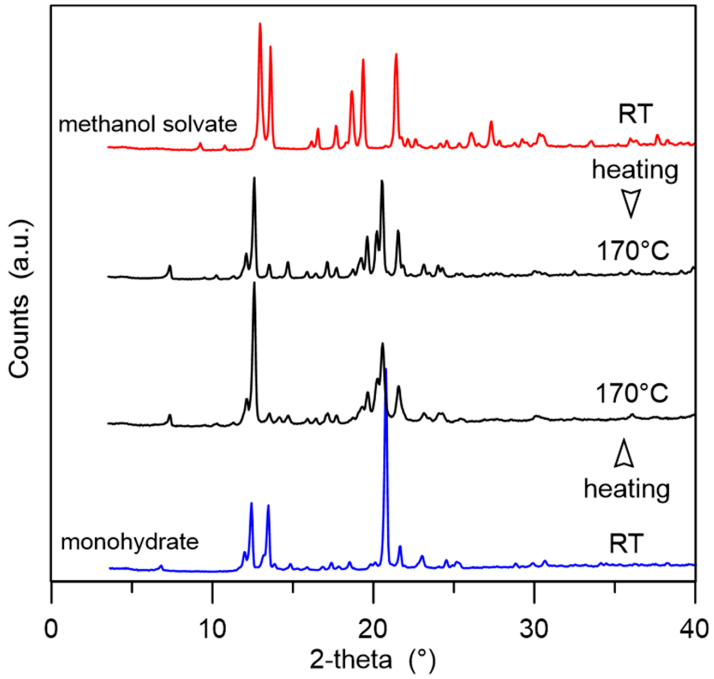

Figure 3. In situ XRD scans before and after thermal evolution of Estetrol.0.5CH_3OH (top) and Estetrol.H_2O (bottom).

The heating was stopped at 170 °C, i.e., at a temperature intermediate between the first TG step, which corresponds to the complete exhaling of solvent molecules and the melting process. At this temperature, the patterns of both solvates are modified and turned into a different one, but identical, regardless of the solvent present in the original sample. By comparison with the pattern reported in the patent literature [27], it can be attributed to an anhydrous form of estetrol. The peak positions and relative intensities recorded at RT are reported in Table 2 as a reference for phase identification. The full set of reflections is the same independently of the starting pseudopolymorphs, but the product coming from the methanol solvate showed sharper peaks, suggesting it has bigger crystal domains; i.e., crystals formed better.

Table 2. Position on the two-theta scale, d-spacings and relative intensities (only peaks ≥ 2%) of estetrol anhydrous obtained from methanol solvate by heating the sample at 170 °C, scanned at RT.

Pos. [°2θ]	d-Spacing [Å]	Rel. Int. [%]	Pos. [°2θ]	d-Spacing [Å]	Rel. Int. [%]
7.352	12.0147	12	23.652	3.7587	3
10.335	8.5528	3	24.319	3.6570	10
11.396	7.7585	2	25.371	3.5077	2
12.216	7.2398	17	25.645	3.4709	3
12.677	6.9774	100	27.091	3.2888	2
13.622	6.4952	11	27.466	3.2448	2
14.780	5.9889	12	27.874	3.1982	3
15.985	5.5398	4	30.415	2.9365	7
16.508	5.3655	3	30.781	2.9024	2
17.260	5.1336	16	32.571	2.7469	2
17.788	4.9823	6	36.197	2.4796	3
18.797	4.7171	5	37.636	2.3881	4
19.207	4.6172	9	37.933	2.3700	2
19.486	4.5519	16	39.194	2.2966	2
19.832	4.4733	35	39.916	2.2568	5
20.433	4.3430	42	40.392	2.2312	3
20.769	4.2735	92	41.497	2.1744	2
21.771	4.0790	32	42.392	2.1305	2
22.511	3.9464	2	43.059	2.0990	2
23.343	3.8078	12	44.817	2.0207	2

3.4. IR Spectroscopy

A comparison of the ATR-FTIR spectra of estetrol in monohydrate and methanol hemisolvate forms is presented in Figure 4. The spectra show almost a full overlap in the 650–1100 cm^{-1} region. This is obviously due to the presence of the same steroidal parent molecular structure. Moving towards the left side, Estetrol.0.5CH_3OH shows a band at 1103 cm^{-1}, due to the additional contribution of methanol to the C-O stretching peak. Other differences between the two pseudopolymorphs are detected in the 1250–1600 cm^{-1} region. More in detail, in the Estetrol.0.5CH_3OH spectrum, a further peak appears at 1282 cm^{-1} due to the phenolic C-O stretch, and the aromatic C=C stretching at 1609 cm^{-1} is paired with a further peak at 1583 cm^{-1}. Some extra peaks are also observed around 3000 cm^{-1} likely due to the C-H stretching of methanol, as well as the additional broad shoulder at 3250 cm^{-1}, derived from the O-H bending of the solvent. The splitting of the stretching bands of the aromatic moiety of estetrol molecules in methanol solvate could be assigned to the presence of solvent molecules disordered over two positions as discussed in the light of single-crystal data in Section 3.6.

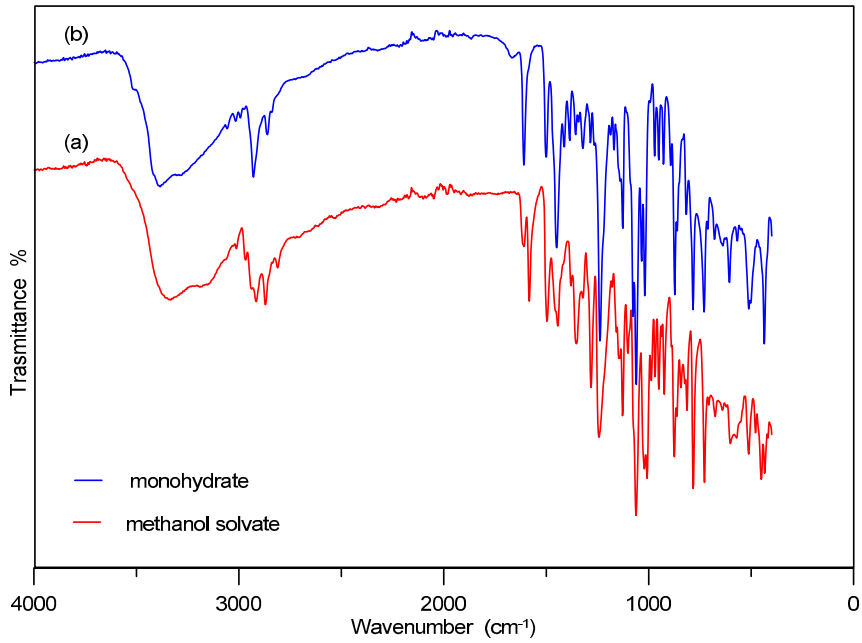

Figure 4. ATR−FTIR spectra for samples of Estetrol.H_2O (**a**) and Estetrol.0.5CH_3OH (**b**).

3.5. Morphology

Single crystals of Estetrol.H_2O were prepared via the slow evaporation of a 2-propanol–water solution of the API, while single crystals of Estetrol.0.5CH_3OH solid were prepared via the slow evaporation of a methanol solution. The two procedures provide crystals of different shapes and sizes as shown in Figure 5.

The hydrate crystals are thin blades ten microns wide but with a length/width ratio in the range of 5 ÷ 10. The methanol solvates are significantly larger with an irregular hexagonal prism shape, but always aggregated and with the presence of several intergrowth crystals.

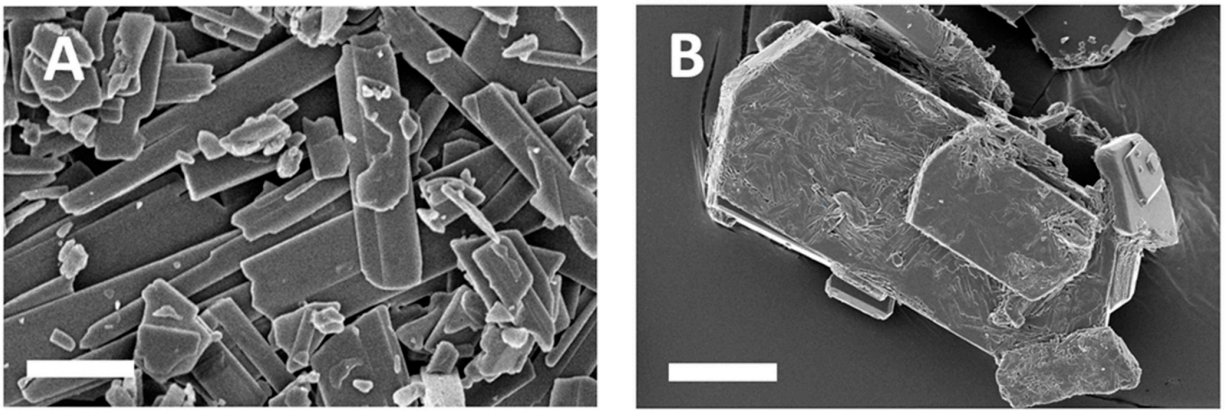

Figure 5. SEM images of Estetrol.H_2O ((**A**), scale bar 10 μm) and Estetrol.0.5CH_3OH ((**B**), scale bar 80 μm).

3.6. Structures Description

The two pseudopolymorphs, Estetrol.H_2O and Estetrol.0.5CH_3OH, crystallize in the triclinic space group *P*1 and monoclinic space group *C*2, respectively, with the parameters reported in Table 1. Interestingly the unit cell of the monohydrate crystal of Estetrol.H_2O contains twelve independent molecules and twelve water molecules (in Figure 6, one molecule is reported as an example, and in Figure 7, the full packing). In the literature, the number of molecules that crystallize with large Z′ values is increasing [36,37] and among steroids, cholesterol, for example, is well known for its propensity to have asymmetric units containing multiple molecules in its solvates [38]. Among the factors that determine the presence of more than one molecule in the asymmetric unit, the formation of several H-bonds is one of the most common, and in the monohydrate estetrol, the presence of four hydroxyl groups is also accompanied by the possibility of involving the water molecules in the O-H. . .O H-bonding network. The twelve molecules of estetrol show very subtle differences with one another, mostly in the conformation of the rings and in the positions of the hydroxyl oxygens.

A close examination of the O-H. . .O hydrogen bonding of each molecule (Table S1) reveals an intricated network made of intermolecular H-bonds established with the neighbour estetrol molecules and with the crystallization water. These O-H...O interactions vary from one molecule to another, and, although the water hydrogens could not be located, pairs of short Ow. . .Ow interactions (2.85 Å) indicate the presence of other O_w-H. . .O_w H-bonds reinforcing the crystal packing. The crystal packing (Figure 7) shows that the conformers form columns, each containing a pair of alternating conformers (shown with different colours) and are organized in a head-to-tail arrangement that favours the formation of O-H. . .O interactions.

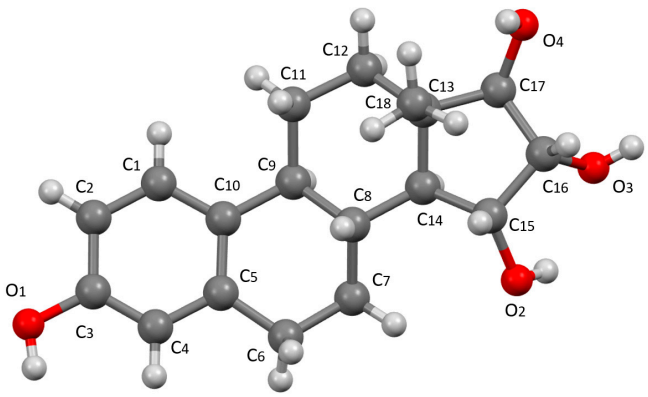

Figure 6. One of the twelve independent molecules of Estetrol.H_2O as an example of molecular conformation.

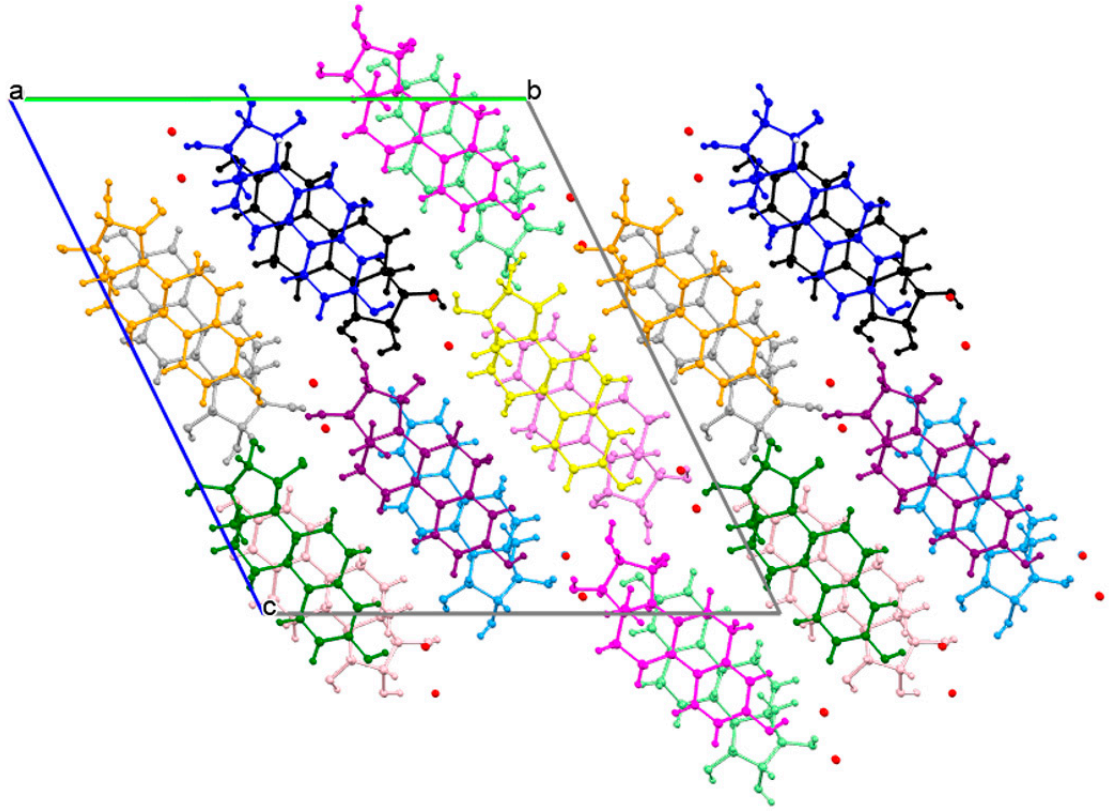

Figure 7. View down the *a*-axis of the crystal packing of Estetrol.H_2O. The 12 independent molecules are represented with different colours.

The conformation of estetrol in Estetrol.0.5CH_3OH is similar to that of the hydrate shown in Figure 6. The asymmetric unit of the second pseudopolymorph, in addition to one molecule of estetrol, contains methanol that lies around a C_2 axis (carbon atom on the axis and oxygen in two positions replicated by symmetry, each one occupied by 1/2). Each molecule of estetrol establishes six O-H. . .O bonds with six different neighbours (Figure 8) and one more H-bond with the disordered methanol molecule. This interaction involves the phenolic hydroxyl with O1. . .Ow distances at 2.64 or 2.79 Å.

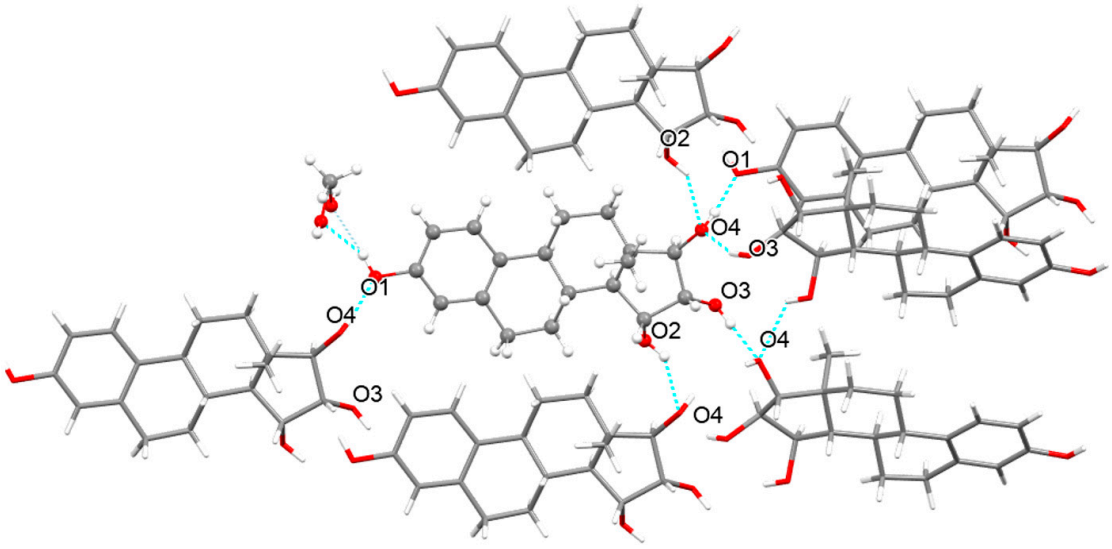

Figure 8. Arbitrary view of the environment of one molecule of Estetrol.0.5CH_3OH (ball and stick style) showing the O-H. . .O H-bonding (dotted light blue lines) with its neighbours.

The crystal packing of Estetrol.0.5CH_3OH (Figure 9) shows that the molecules are arranged in columns in a head-to-tail orientation, whereas the methanol runs along the *a*-axis. The estetrol columns are connected to each other through intermolecular O-H. . .O hydrogen bonds (Table S2).

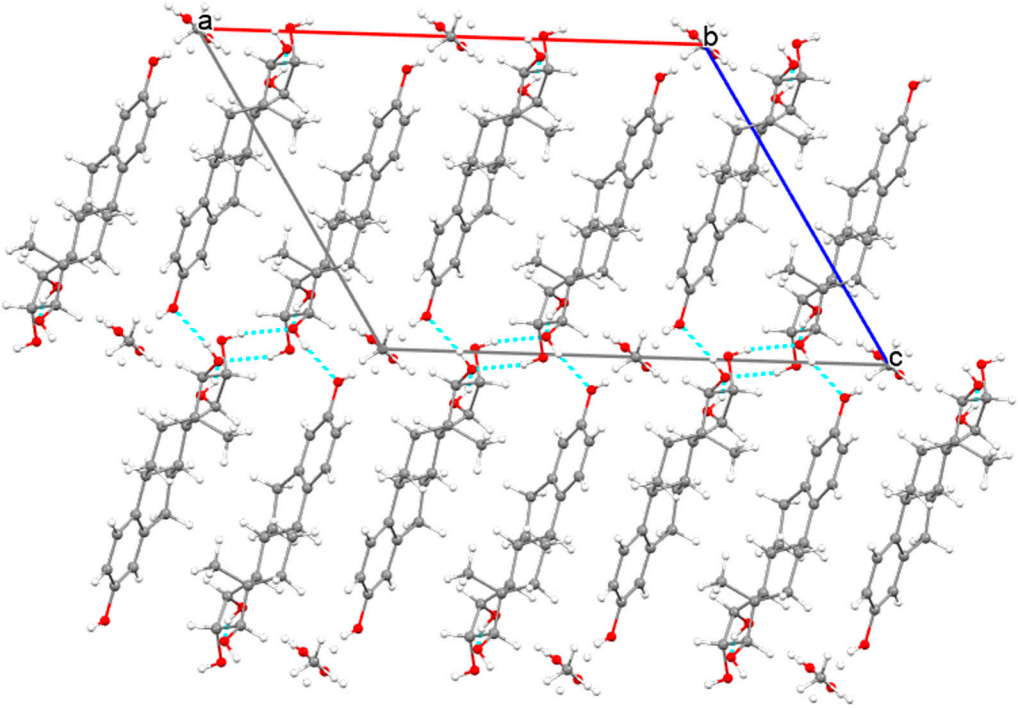

Figure 9. View down the *b*-axis of the crystal packing of Estetrol.0.5CH_3OH. Dotted light blue lines indicate O-H. . .O hydrogen bonding.

This head-to-tail arrangement is also present in the solid-state structure of other estrogenic steroids such as Estriol (E3) [39] that crystallize without a crystallization solvent and 17-β-estradiol (E2). The latter has been structurally characterized several times in solvates, hydrated solid forms and, more recently, without a crystallization solvent [40,41]. In the methanol hemisolvate form, the packing motif of E2 is similar to that adopted in the estetrol pseudopolymorphs like the role of the solvent as a linker of the chains of the steroid through O-H. . .O H-bonding.

To ascertain that single crystals investigated for structural characterization well represent the whole batches used in the powder and thermal investigations, XRD powder patterns calculated from crystallographic data were compared with those experimentally obtained from powder samples. The good reproduction of Estetrol.0.5CH_3OH and Estetrol.H_2O profiles, reported in Figure 2b,d, respectively, confirm this hypothesis and improves its relevance to the crystallographic study.

4. Conclusions

Two pseudopolymorphs of estetrol have been crystallized allowing for the first time structure determination of the E4 hormone. In both structures, molecules are arranged in a head-to-tail assembly which provides an intricate network of hydrogen bonds with the participation of a crystallization solvent. The splitting of the C=C stretches in the ATR-FTIR spectrum of Estetrol.0.5CH_3OH confirms the relevant interaction of the estetrol molecule with methanol. The identification of stable Estetrol.0.5CH_3OH can represent a clear benefit if applied to the purification process of the estetrol in order to meet the ICH [42] specifications for related substances. Indeed, organic impurities usually precipitate together with the crystals of the API in the presence of water, while from methanol, clean purification takes place during crystallization. Furthermore, thermal stability is increased in

Estetrol.0.5CH_3OH with respect to Estetrol.H_2O crystals. Even though, in terms of the initial objectives, we successfully discovered a new crystalline form of estetrol, in our laboratory, the in-depth exploration of the solid state of estetrol is still ongoing, with the aim of finding new pseudopolymorphs and expanding the possibility of choosing the crystallization which will definitively enable the best industrial purification of crude estetrol. Currently, both alcoholic solvents such as isopropanol and THF are under investigation, and the results will be given in due course.

Supplementary Materials: The following supporting information can be downloaded at: https://www.mdpi.com/article/10.3390/cryst13081211/s1, Table S1: Intermolecular and intramolecular hydrogen bonds for Estetrol.H_2O; Table S2: Intermolecular hydrogen bonds for Estetrol.0.5CH_3OH.

Author Contributions: Conceptualization, E.A., M.G. and M.M.; Synthesis, E.A., G.L. and F.B.; Thermal scouting, M.G. and M.M.; Spectroscopic investigation, E.A., G.L. and F.B.; Structure investigation, M.G. and M.M. All authors have read and agreed to the published version of the manuscript.

Funding: This research received no external funding.

Data Availability Statement: Not Applicable.

Acknowledgments: M.M. acknowledges University of Bologna for RFO funds.

Conflicts of Interest: The authors declare no conflict of interest.

References

1. Zucconi, G.; Lisboa, B.P.; Simonitsch, E.; Roth, L.; Hagen, A.A.; Diczfalusy, E. Isolation of 15α-hydroxy-oestriol from pregnancy urine and from the urine of newborn infants. *Eur. J. Endocrinol.* **1967**, *56*, 413–423. [CrossRef] [PubMed]
2. Hagen, A.A.; Barr, M.; Diczfalusy, E. Metabolism of 17β-oestradiol-4-14c in early infancy. *Eur. J. Endocrinol.* **1965**, *49*, 207–220. [CrossRef]
3. Holinka, C.F.; Diczfalusy, E.; Herjan, J.T.; Coelingh Bennink, H.J. Estetrol: A unique steroid in human pregnancy. *J. Steroid Biochem. Mol. Biol.* **2008**, *110*, 138–143. [CrossRef] [PubMed]
4. Bennink, H.J.T.C.; Holinka, C.F.; Diczfalusy, E. Estetrol review: Profile and potential clinical applications. *Climacteric* **2008**, *11*, 47–58. [CrossRef]
5. Visser, M.; Holinka, C.F.; Bennink, H.J.T.C. First human exposure to exogenous single-dose oral estetrol in early postmenopausal women. *Climacteric* **2008**, *11* (Suppl. S1), 31–40. [CrossRef]
6. Visser, M.; Bennink, H.J.C. Clinical applications for estetrol. *J. Steroid Biochem. Mol. Biol.* **2009**, *114*, 85–89. [CrossRef]
7. Morimont, L.; Haguet, H.; Dogné, J.-M.; Gaspard, U.; Douxfils, J. Combined Oral Contraceptives and Venous Thromboembolism: Review and Perspective to Mitigate the Risk. *Front. Endocrinol.* **2021**, *12*, 769187. [CrossRef]
8. Douxfils, J.; Morimont, L.; Bouvy, C. Oral Contraceptives and Venous Thromboembolism: Focus on Testing that May Enable Prediction and Assessment of the Risk. *Semin. Thromb. Hemost.* **2020**, *46*, 872–886. [CrossRef]
9. Gérard, C.; Blacher, S.; Communal, L.; Courtin, A.; Tskitishvili, E.; Mestdagt, M.; Munaut, C.; Noël, A.; Gompel, A.; Pequeux, C.; et al. Estetrol is a weak estrogen antagonizing estradiol-dependent mammary gland proliferation. *J. Endocrinol.* **2015**, *224*, 85–95. [CrossRef]
10. Mawet, M.; Maillard, C.; Klipping, C.; Zimmerman, Y.; Foidart, J.-M.; Bennink, H.J.T.C. Unique effects on hepatic function, lipid metabolism, bone and growth endocrine parameters of estetrol in combined oral contraceptives. *Eur. J. Contracept. Reprod. Health Care* **2015**, *20*, 463–475. [CrossRef]
11. Fruzzetti, F.; Fidecicchi, T.; Guevara, M.M.M.; Simoncini, T. Estetrol: A New Choice for Contraception. *J. Clin. Med.* **2021**, *10*, 5625. [CrossRef] [PubMed]
12. Estetra, S.P.R.L. A Randomized Double-Blind Placebo Controlled Phase 3 Trial to Evaluate the Efficacy and Safety of Estetrol for the Treatment of Moderate to Severe Vasomotor Symptoms in Postmenopausal Women (E4Comfort Study I). EUDRACT 2019-001289-14; ClinicalTrials.gov Identifier: NCT04209543. Available online: https://classic.clinicaltrials.gov/ct2/show/NCT04209543 (accessed on 23 July 2023).
13. Estetra, S.P.R.L. A Randomized Double-Blind Placebo Controlled Phase 3 Trial to Evaluate the Efficacy and Safety of Estetrol for the Treatment of Moderate to Severe Vasomotor Symptoms in Postmenopausal Women (E4Comfort Study II). ClinicalTri-als.gov Identifier: NCT04090957. Available online: https://classic.clinicaltrials.gov/ct2/show/NCT04090957 (accessed on 23 July 2023).
14. Utian, W.H.; Lobo, R.; Mawet, M. A phase 3 protocol to assess the efficacy and safety of estetrol (E4), a promising new treatment for menopausal vasomotor symptoms. *Menopause* **2019**, *26*, 1480.
15. Gaspard, U.; Taziaux, M.; Jost, M.; Skouby, S.O.; Lobo, R.A.; Foidart, J.-M. Estetrol (E4), the next generation hormone therapy (HT) for menopausal symptoms: Phase 2b clinical trial results. In Proceedings of the 12th European Congress on Menopause and Andropause, Berlin, Germany, 15–17 May 2019; Lippincott Williams & Wilkins: Philadelphia, PA, USA, 2019; Volume 124, p. 9. [CrossRef]

16. Gaspard, U.; Taziaux, M.; Mawet, M.; Jost, M.; Gordenne, V.; Bennink, H.J.T.C.; Lobo, R.A.; Utian, W.H.; Foidart, J.-M. A multicenter, randomized study to select the minimum effective dose of estetrol (E4) in postmenopausal women (E4Relief): Part 1. Vasomotor symptoms and overall safety. *Menopause* **2020**, *27*, 848–857. [CrossRef] [PubMed]
17. Schmidt, M.; Lenhard, H.; Hoenig, A.; Zimmerman, Y.; Krijgh, J.; Jansen, M.; Bennink, H.J.T.C. Tumor suppression, dose-limiting toxicity and wellbeing with the fetal estrogen estetrol in patients with advanced breast cancer. *J. Cancer Res. Clin. Oncol.* **2021**, *147*, 1833–1842. [CrossRef] [PubMed]
18. Mithra Pharmaceuticals' Estetrol Programs. Available online: https://www.mithra.com/en/estetrol/ (accessed on 18 July 2023).
19. Available online: https://www.acs.org/molecule-of-the-week/archive/e/estetrol.html (accessed on 18 July 2023).
20. Platteeuw, J.J.; Coelingh, B.H.; Damen, F.W.; Van Vliet, M.C. Process for the Preparation of Estetrol. WO Patent 2013/012328A1, 24 January 2013.
21. Pascal, J.C. Process for the production of Estetrol. WO Patent 2013/050553A1, 11 April 2013.
22. Ferreiro Gil, J.J.; Iglesias Retuerto, J.M.; Gallo Nieto, F.J. Process for the preparation of Estetrol and Related Compounds. WO Patent 2013/034780A2, 3 October 2013.
23. Lovas, R.; Mahò, S.; Bacsa, I.; Mayer, B. Industrial Process for the Preparation of High Purity Estetrol. WO Patent 2021044302A1, 11 March 2021.
24. Fabris, F.; Farinella, F.; Gambarin, L.; Merlo, M.; Lopopolo, G.; Attolino, E. Processes for the Preparation of Estetrol and Intermediates Thereof. WO Patent 2023/001866A1, 26 January 2023.
25. Schallmey, A.; Schrepfer, P.; Fuchs, H.; Seeger, M.; Marechal, D.; Cornet, F. Means and Methods for the Conversion of Estradiol to 15alpha-Hydroxyestradiol. WO Patent 2022/074001A1, 14 April 2022.
26. Bianchi, P.; Dubart, A.; Moors, M.; Cornut, D.; Duhirwe, G.; Ampurdanés, J.; Monbaliu, J.-C.M. Metal-free synthesis of estetrol key intermediate under intensified continuous flow conditions. *React. Chem. Eng.* **2023**, *8*, 1565–1575. [CrossRef]
27. Platteeuw, J.J.; Coelingh Bennink, H.J.; Donesta Bioscience, B.V. Orally Disintegrating Solid Dosage Unit Containing an Estetrol Component. WO Patent 2015/086643A1, 18 July 2015.
28. Nambara, T.; Sudo, K.; Kurata, M.S. Syntheses of estetrol monoglucuronides. *Steroids* **1976**, *27*, 111–122. [CrossRef]
29. *APEX3 Software Package*, V2019; Bruker AXS Inc.: Madison, WI, USA, 2019.
30. *Bruker SAINT, v8.40A: Part of the APEX3 Software Package*, V2019; Bruker AXS Inc.: Madison, WI, USA, 2019.
31. *Bruker SADABS V2016/2: Part of the APEX3 Software Package*, V2019; Bruker AXS Inc.: Madison, WI, USA, 2019.
32. Sheldrick, G.M. SHELXT—Integrated Space-Group and Crystal-Structure Determination. *Acta Crystallogr. Sect. A Found. Adv.* **2015**, *71*, 3–8. [CrossRef]
33. Sheldrick, G.M. Crystal structure refinement with *SHELXL*. *Acta Crystallogr. Sect. C Struct. Chem.* **2015**, *71*, 3–8. [CrossRef]
34. Macrae, C.F.; Bruno, I.J.; Chisholm, J.A.; Edgington, P.R.; McCabe, P.; Pidcock, E.; Rodriguez-Monge, L.; Taylor, R.; Streek, J.; van de Wood, P.A. Mercury CSD 2.0—New Features for the Visualization and Investigation of Crystal Structures. *J. Appl. Crystallogr.* **2008**, *41*, 466–470. [CrossRef]
35. Cambridge Crystallographic Database. Available online: https://www.ccdc.cam.ac.uk/structures/ (accessed on 23 July 2023).
36. Steed, K.M.; Steed, J.W. Packing Problems: High Z′ Crystal Structures and Their Relationship to Cocrystals, Inclusion Com-pounds, and Polymorphism. *Chem. Rev.* **2015**, *115*, 2895–2933. [CrossRef]
37. Brock, C.P. High-Z' structures of organic molecules: Their diversity and organizing principles. *Acta Crystallogr. Sect. B Struct. Sci.* **2016**, *72*, 807–821. [CrossRef] [PubMed]
38. Hsu, L.-Y.; Kampf, J.W.; Nordman, C.E. Structure and pseudosymmetry of cholesterol at 310 K. *Acta Crystallogr. Sect. B Struct. Sci.* **2002**, *58*, 260–264. [CrossRef] [PubMed]
39. Cooper, A.; Norton, D.A.; Hauptman, H. Estrogenic steroids. III. The crystal and molecular structure of estriol. *Acta Crystallogr. Sect. B Struct. Crystallogr. Cryst. Chem.* **1969**, *25*, 814–828. [CrossRef] [PubMed]
40. Parrish, D.A.; Pinkerton, A.A. Estradiol methanol hemisolvate. *Acta Crystallogr Sect. C Struct. Chem.* **1999**, *C55*, IUC9900100. [CrossRef]
41. Stevenson, E.L.; Lan-caster, R.W.; Buanz, A.B.M.; Price, L.S.; Tocher, D.A.; Price, S.L. The solid state forms of the sex hormone 17-β-estradiol. *Cryst. Eng. Comm.* **2019**, *21*, 2154–2163. [CrossRef]
42. The International Council for Harmonisation of Technical Requirements for Pharmaceuticals for Human Use. *Quality Guidelines (Q3A–Q3E)*; ICH: Geneva, Switzerland. Available online: https://pharmaguddu.com/ich-guidelines-in-pharmaceutical-updated/ (accessed on 23 July 2023).